Organometallic Polymers with the Backbone Consisting of Ferrocene and Bimetallic Tetracarboxylates

Wen-Mei Xue,[a] Fritz E. Kühn,*[a] Eberhardt Herdtweck,[a] and Quanchang Li[a]

Keywords: Ferrocene / Molybdenum / Multiple bonds / Oligomers / Rhodium

The tetranuclear compounds $Mo_2(O_2CCF_3)_4(FPA)_2$ (**1**), $Rh_2(O_2CCH_3)_4(FPA)_2$ (**2**), and $Rh_2(O_2CCF_3)_4(FPA)_2$ (**3**) (FPA = ferrocenyl-4-pyridylacetylene) have been synthesized by the reaction of bimetallic tetraacetates with FPA in a 1:2 stoichiometry. They have been investigated as models of oligomeric and polymeric complexes of analogous composition. UV/Vis absorption spectroscopy and cyclic voltammetry indicate that $Rh_2(O_2CCF_3)_4$ possesses the strongest inductive effect of the three bimetallic tetracarboxylates examined in this study. Complex **1** was additionally characterized by single crystal X-ray analysis, revealing a Mo–Mo distance of 214.22(3) pm, which is elongated in comparison to $Mo_2(O_2CCF_3)_4$ [209.0(4) pm], and a Mo–N distance of 250.4(2) pm. Oligomers with backbones consisting of 1,1′-bis(4-pyridylethynyl)ferrocene (BPEF) and bimetallic tetracarboxylates, $[M_2(O_2CR)_4(BPEF)]_n$ (M = Mo, R = CF_3, **4**; M = Rh, R = CH_3, **5**; M = Rh, R = CF_3, **6**), have been prepared by treating the bimetallic tetracarboxylates with BPEF in a 1:1 molar ratio. The terminal groups and the number of repeating units have been estimated by elemental analyses. The oligomeric complexes **5** and **6** are insoluble in all common solvents. Complex **4** dissolves in strongly coordinating donor solvents due to replacement of the BPEF ligands by solvent molecules.

Introduction

Polymers and oligomers containing metal-metal bonds in the backbone may display novel conductive, optical, and magnetic properties.[1] A number of bimetallic carboxylates[1f,2a] have been linked by bidentate axial ligands, resulting in one-dimensional polymeric species. Pyrazine has been used to link $Cr_2(O_2CCH_3)_4$,[2b] $Mo_2(O_2CCH_3)_4$,[3a] $Cu_2(O_2CCH_3)_4$,[3b] and $Ru_2\{O_2C(CH_2)_6CH_3\}_4$.[3c] $Mo_2(O_2CCF_3)_4$ units have been linked by 9,10-anthraquinone, 2,6-dimethyl-1,4-benzoquinone, 1,4-naphthoquinone,[3d] and 2,5-dimethyl-*N*,*N*′-dicyanoquinone diimine (2,5-DM-DCNQI).[3e] $Mo_2(O_2CCH_3)_4$ units have been bridged by 4,4′-bipyridine,[3a] 1,2-bis(dimethylphosphanyl)ethane (dmpe) and tetramethylethylenediamine (tmed).[3f] $Rh_2(O_2CC_2H_5)_4$ units have been linked by phenazine and durenediamine ligands, respectively.[2c] Phenazine has also been employed to connect cationic $Ru_2(O_2CC_2H_5)_4^+$ complexes to afford polymers.[2d] However, to the best of our knowledge, examples of oligomers and polymers based on bimetallic monomers with organometallic spacing groups are not yet known in the literature.[1f] This paper describes the first representatives of bimetallic oligomers bridged by π-conjugated ferrocene derivatives. $Mo_2(O_2CCF_3)_4$ is feasible as a building block because, in principle, the quadruple bond allows a delocalization of electrons along the oligomer chain. Dirhodium tetracarboxylates $Rh_2(O_2CCH_3)_4$ and $Rh_2(O_2CCF_3)_4$ are also employed, taking advantage of their air- and moisture-stability. The replacement of CH_3 by CF_3 is recommended for increasing the solubility and the metal-axial ligand interaction in the oligomer.

Ferrocene-containing complexes are currently receiving much attention due to their increasing role in the rapidly growing area of materials science. They have been of use as charge-transfer complexes and polymers,[4] molecular sensors,[5] and in nonlinear optics.[6] The favorable electrochemical properties of ferrocene make this molecule a particularly promising candidate for incorporation into polymer chains. It is quite obvious that ferrocene polymers are more likely to display exceptional properties when the different metal centers are intimately coupled through suitable unsaturated bridging units.[7] We therefore explore an oligomer system containing both ferrocene and metal-metal bonds in the backbone. Introduction of bimetallic complexes into the ferrocene-based oligomers combines the advantages of both the ferrocene and the metal-metal bonds. Additionally, it allows the use of a wider diversity of metals (Mo, Rh, Re, Cu, Cr, W, Pt, Ru, etc.) and equatorial ligands which may be helpful in fine-tuning the oligomer properties.

Results and Discussion

Tetranuclear Complexes

Preparation and Characterization

In order to better understand the electronic and electrochemical properties of oligomeric complexes of analogous composition, complexes **1**–**3** were synthesized as models by the reaction of dirhodium- or dimolybdenum-tetracarboxylate with the monodentate FPA ligand in a 1:2 molar ratio as shown in Equation (1).

[a] Anorganisch-Chemisches Institut der Technischen Universität München,
Lichtenbergstraße 4, 85747 Garching bei München, Germany
Fax: (internat.) +49-89/289-13473
E-mail: fritz.kuehn@ch.tum.de

  1434–1948/01/0101–0213 $ 17.50+.50/0

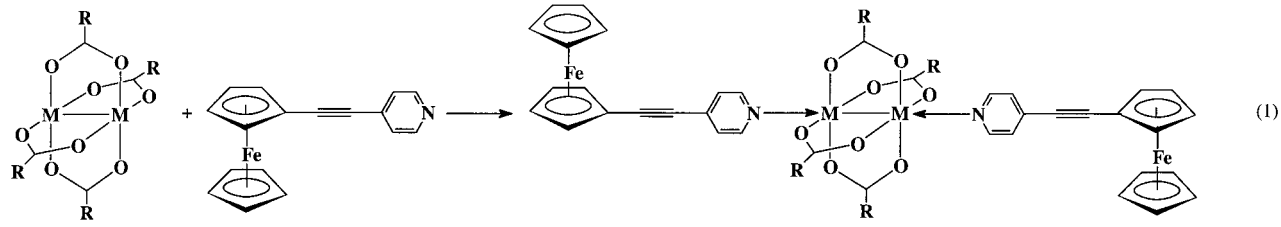

FPA

	M	R
1	Mo	CF_3
2	Rh	CH_3
3	Rh	CF_3

(1)

The dimolybdenum compound **1** decomposes when exposed to air within a couple of hours in the solid state and within 10 minutes in solution. The dirhodium complexes **2** and **3** are air stable. Compounds **1** and **3** are soluble in most polar organic solvents, e.g. CH_2Cl_2, $CHCl_3$, MeCN, THF, etc., but **2** is only soluble in CH_2Cl_2 and $CHCl_3$, due to the commonly lower solubility of acetyl complexes in comparison to trifluoroacetyl compounds.[2a]

The IR active C≡C stretching vibration gives rise to bands at 2207, 2205, and 2206 cm^{-1} respectively for compounds **1**–**3**. This vibration is slightly lower in energy in all cases than in the free FPA ligand (2210 cm^{-1}). The pyridyl ring stretching vibration appears at 1601, 1603, and 1604 cm^{-1}, the corresponding signal of FPA at 1594 cm^{-1}.

The pyridyl protons of **2** [$\delta(H_\alpha)$ = 9.11, $\delta(H_\beta)$ = 7.72] show their resonances at lower field than the free ligand FPA (δ = 8.53 and 7.32, respectively). In contrast, up-field shifts of the α-ring pyridyl protons are observed in compounds **1** (δ = 8.03) and **3** (δ = 8.27), possibly due to the strong electron-withdrawing effect of the trifluoroacetyl ligands, which diminish backbonding effects from the bimetallic cores. The ferrocene proton resonances are comparable for compounds **1**–**3** and the free ligand. The proton NMR signal of the CH_3CO_2 group is shifted downfield in CD_2Cl_2 from δ = 1.76 [axial ligand free $Rh_2(O_2CCH_3)_4$] to δ = 1.88 in the case of complex **2**, demonstrating that electron density must be shifted back to the ferrocenyl unit in the latter molecule. The ^{13}C NMR spectroscopic data of the CH_3 moiety shows the same trend [δ = 23.5 in the starting material $Rh_2(O_2CCH_3)_4$ and δ = 30.1 in the axially ligated product compound].

Attempts to prepare mixed-valence complexes by chemical oxidation have not yet been successful. Treatment of $Rh_2(O_2CCH_3)_4(FPA)_2$ with I_2 in dichloromethane at room temperature resulted in no reaction, while the same treatment carried out on $Mo(O_2CCF_3)_4(FPA)_2$ led to immediate decomposition.

Structural Investigation

The molecular structure of compound **1** together with selected interatomic distances, angles and torsion angles are shown in Figure 1. The neutral complex crystallizes in the space group *P*1(bar) (No. 2). Quadruply bonded dimolybdenum complexes with four bridging $(O_2CCF_3)^-$ ligands usually exhibit a crystallographic center of inversion in the solid state, as does compound **1**. The two pyridyl ligands coordinate to the molybdenum atoms in the axial positions and are slightly bent [Mo_a–Mo–N 165.85(5)°]. Compound **1** and all other 11 crystallographically characterized compounds with a $[Mo_2(\mu\text{-}O_2CCF_3)_4]$ building block exhibit a very similar core geometry.[8] As expected the $[Mo_2(\mu\text{-}O_2CCF_3)_4]$ unit has a nearly idealized D_{4h} symmetry. The observed Mo–Mo bond length of 214.22(3) pm in **1** is found at the upper end of the known range for Mo–Mo quadruple bonds. The elongation of the Mo–Mo bond in comparison to the starting material {$[Mo_2(\mu\text{-}O_2CCF_3)_4]$, *d*(MoMo) = 209.0(4) pm} is clearly due to the electron donor capability of the axial ligands. Donation of additional electron density to a quadruple bond leads to a weakening of the Mo–Mo interaction, caused by the involvement of antibonding orbitals. The Mo–O distances do not vary significantly. The Mo-pyridyl bond is comparatively long [Mo–N 250.4(2) pm], indicating relatively weak molybdenum–nitrogen interactions. However, the Mo–N distance is shorter than expected from the sum of the van der Waals radii (Mo–N: 382 pm) but longer than the sum of the covalent radii (Mo–N: 215 pm).[8] The NMR and IR data described above are in good agreement with all these observations.

Electronic Absorption Spectra

Any perturbation of the electronic structure of the ferrocenes should lead to a bathochromic shift of the respective UV/Vis transitions. Figure 2 presents a comparison of the UV/Vis spectra of complex **2** and FPA. A peak at 365 nm (13600 M^{-1} cm^{-1}) and a broad band around 451 nm (3040 M^{-1} cm^{-1}) in **2** are assigned to d-d transitions in the ferrocene unit.[9] FPA shows similar absorptions at 352 nm (2320 M^{-1} cm^{-1}) and 449 nm (760 M^{-1} cm^{-1}) but significantly lower extinction coefficients. The higher energy d-d transition bands in the spectra of complexes **1** and **3** are probably shoulders of π-π* absorptions. As shown in Table 1, the lower energy absorptions appear around 451 nm (2340 M^{-1} cm^{-1}) and 466 nm (6310 M^{-1} cm^{-1}) in the derivatives **1** and **3**. In addition to the d-d transitions, the spectra show a strong peak assigned to a π-π* transition at about 310 nm: FPA, 304 nm (12800 M^{-1} cm^{-1}); **1**, 305 (37499); **2**, 308 (32800); **3**, 316 (47500). The shift to longer wavelength absorptions in the case of derivatives **1**–**3** compared to unco-

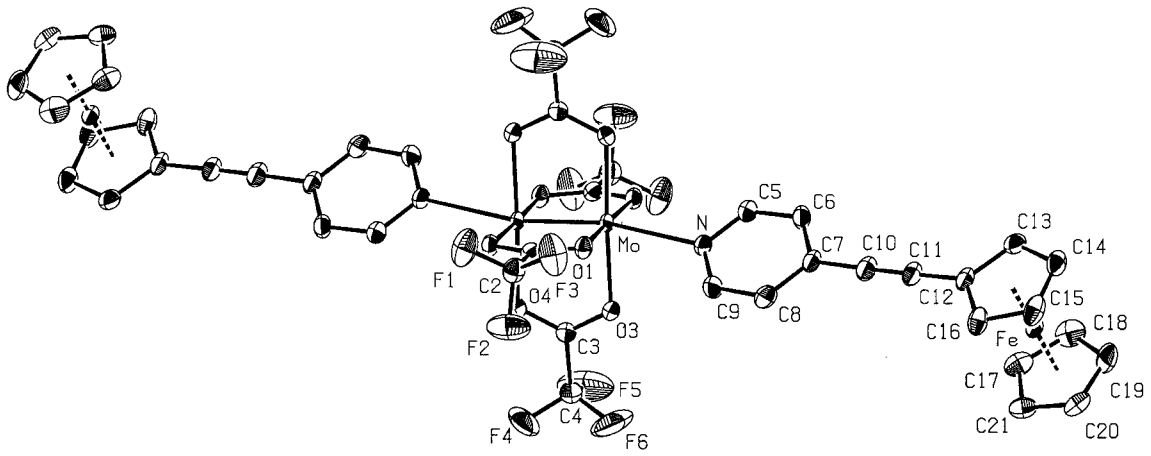

Figure 1. ORTEP drawing of the molecular structure of **1** in the solid state; thermal ellipsoids are at the 50% probability level; hydrogens omitted for clarity; selected bond lengths [pm], angles and torsion angles [°]: Mo−Mo_a 214.22(3), Mo−O1 214.45(19), Mo−O3 213.6(2), Mo_a−O2 211.22(19), Mo_a−O4 211.6(2), Mo−N 250.4(2), C10−C11 120.0(4); O1−Mo−$O2_a$ 177.25(7), O3−Mo−$O4_a$ 177.26(7), O1−Mo−O3 91.23(7), O1−Mo−$O4_a$ 88.19(7), $O4_a$−Mo−$O2_a$ 91.58(7), $O2_a$−Mo−O3 88.87(7), Mo_a−Mo−N 165.85(5); O1−Mo−Mo_a−O2 −0.09(7), O3−Mo−Mo_a−O4 −0.61(7); translation of symmetry code to equivalent positions: $a = 1 - x, 2 - y, -z$

ordinated FPA is probably due to the inductive effects of the dimetallic moieties. The degree of deviation of the bathochromic shifts of both d-d and π-π* transitions of complex **3** vs. FPA are bigger than in the case of compound **2**, due to the strong electron-withdrawing effect of the trifluoroacetyl groups. Complexes **1** and **3** bear the same carboxylato ligand, but the shifts of both d-d and π-π* bands in **3** vs. FPA are more pronounced than in derivative **1**. This reflects the fact that the Lewis acidity of $Rh_2(O_2CCF_3)_4$ is higher than that of $Mo_2(O_2CCF_3)_4$.

Electrochemical Properties

As depicted in Figure 3, the cyclic voltammogram of complex **2** in CH_2Cl_2 exhibits two subsequently reversible anodic couples. The first oxidation with $E_{1/2} = 0.18$ V is assigned to the oxidation of the two ferrocene units, whereas the second with $E_{1/2} = 0.52$ V is due to the oxidation process $[Rh_2]^{5+/4+}$. The coordination of dirhodium(II) by FPA results in a pronounced cathodic shift of $[Rh_2]^{5+/4+}$ from the parent $Rh_2(O_2CCH_3)_4$ (0.90 V), probably due to the strong electron-donating ability of FPA. The weak anodic shift of $Fe^{3+/2+}$ in complex **2** compared to FPA (0.12 V) is probably caused by the inductive effect of the acetate ligands in $Rh_2(O_2CCH_3)_4$. This effect compensates at least partially the electron deficiency of the Rh centers. As presented in Table 1, the $Fe^{3+/2+}$ oxidation potentials of **1** and **3** are also anodically shifted to 0.17 V and 0.27 V respectively from the parent FPA. Moreover, the shift of compound **3** vs. free FPA is more remarkable than the one in **1** and **2**, reflecting the negative inductive effect of the trifluoroacetate ligands of $Rh_2(O_2CCF_3)$. This result is consistent with the results obtained from electron absorption spectroscopy (see above).

FPA gives a half-peak width $W_{1/2}$ of 237 mV, whereas complex **1** displays a $W_{1/2}$ of 297 mV. Although the $Fe^{3+/2+}$ oxidation peak width of **1** is 60 mV broader than that of

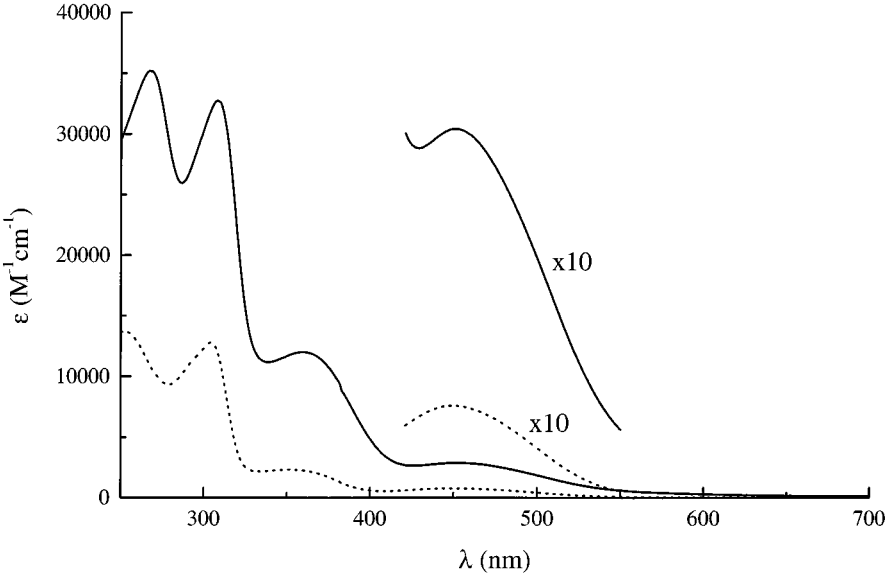

Figure 2. UV/Vis absorption spectra of $Rh_2(O_2CCH_3)_4(FPA)_2$ (**2**, solid line) and FPA (dotted line) in CH_2Cl_2 at room temperature

Table 1. Ferrocene oxidation potentials and electronic absorptions of the complexes and ligands at room temperature

Material	E (ΔE_p)/$Fe^{3+/2+}$ [a]	λ_{max},[b] nm (ε, 10^3 м$^{-1}$ cm^{-1})
$Mo_2(O_2CCF_3)_4(FPA)_2$ **1**	0.17 (80)	305 (37.4), 451 (2.34)
$Rh_2(O_2CCH_3)_4(FPA)_2$ **2**	0.18 (61)	267 (35.2), 308 (32.8), 365 (13.6), 451 (3.04)
$Rh_2(O_2CCF_3)_4(FPA)_2$ **3**	0.27 (62)	260 (6.39), 316 (9.46), 466 (6.31)
$[Mo_2(O_2CCF_3)_4(BPEF)]_n$ **4**	0.41 (61)[c][d] −0.20 (ir)[e]	304 (16.6), 439 (1.19)[c][f]
FPA	0.12 (72)	304 (12.8), 352 (2.32), 449 (0.76)
BPEF	0.43 (ir)[c] −0.22 (ir)[e]	308 (16.9), 350 (3.55), 458 (0.87)[c] 311 (19.6), 350 (4.16), 457 (1.04)

[a] Performed in deoxygenated CH_2Cl_2 solutions except otherwise stated. Potentials in volts vs. ferrocene (0.00 V with ΔE_p = 95 mV in CH_2Cl_2 and 66 mV in CH_3CN). Scan rate is 50 mV/s except otherwise stated. $\Delta E_p = E_{pa} - E_{pc}$ (mV). − [b] Measured in CH_2Cl_2 solutions except otherwise stated. − [c] Measured in CH_3CN. − [d] Scan rate is 200 mV/s. − [e] Measured in THF. − [f] Molarity is based on the repeating unit.

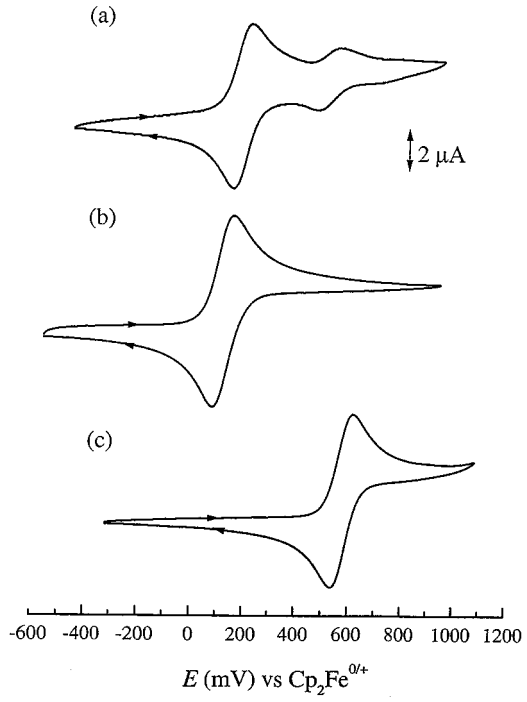

Figure 3. Cyclic voltammograms of (a) $Rh_2(O_2CCH_3)_4(FPA)_2$ (**2**), (b) FPA and (c) $Rh_2(O_2CCH_3)_4$ at the same scan rate of 50 mV/s in CH_2Cl_2 with 0.1 м TBAH at room temperature

FPA, both DPV and SQW measurements reveal a single process. A single $Fe^{3+/2+}$ oxidation wave as narrow as that of FPA is observed for both compounds **2** and **3**. The apparent lack of interaction between the ferrocene units in the tetranuclear complexes might be due to the less favorable energetic positions of the available orbitals in the complexes, the relatively weak Mo-axial ligand interactions and the presence of the rather long conjugating units between the ferrocene fragments.

Thermogravimetry

The complexes **1**−**3** and their precursor complexes $Mo_2(O_2CCF_3)_4$, $Rh_2(O_2CCF_3)_4$, $Rh_2(O_2CCH_3)_4$, and FPA have been examined by thermogravimetry (TG). While the bimetallic starting materials sublime with onset temperatures of 226 °C [$Mo_2(O_2CCF_3)_4$], 278 °C [$Rh_2(O_2CCH_3)_4$], and 312 °C [$Rh_2(O_2CCF_3)_4$], FPA starts to decompose at 229 °C, the tetrameric product complexes **1** and **2** are more stable than both their precursor complexes, with decomposition onset temperatures of 247 °C and 296 °C. However, compound **3** decomposes with a lower onset temperature (275 °C) than its bimetallic precursor $Rh_2(O_2CCF_3)_4$. The product complexes **1**−**3** are therefore in general significantly more stable than the least stable starting material, two of them are even more thermally stable than both precursors. This clearly proves the formation of product compounds of significant stability.

Oligomeric and Polymeric Complexes

Preparation and Characterization

The one-dimensional organometallic oligomer $[Mo_2(O_2CCF_3)_4(BPEF)]_n$ (**4**) with alternating ferrocene units and dimolybdenum quadruple bonds in the π-conjugated chain is obtained by the reaction of $Mo_2(O_2CCF_3)_4$ with one equivalent of BPEF [BPEF = 1,1′-bis(4-pyridylethynyl-)ferrocene] as shown in Equation 2. The orange solid is readily soluble in THF, moderately soluble in CH_3CN, and insoluble in all other common organic solvents. The solid state IR spectrum exhibits the characteristic C≡C stretching vibration at 2211 cm^{-1} and the C−F stretching vibration at 1193 cm^{-1}. These bands are nearly identical in energy to those in free BPEF [ν(C≡C) = 2208 cm^{-1}] and $Mo_2(O_2CCF_3)_4$ [ν(C−F) = 1192 cm^{-1}]. The strong band at 1592 cm^{-1} attributed to the pyridyl ring shifts to 1603 cm^{-1} after ligation.

Elemental analyses are consistent with an oligomer or polymer having the stoichiometry $Mo_2(O_2CCF_3)_4$/BPEF = 1:1. The ^1H NMR spectroscopic data of δ($H_α$-pyridyl) (δ = 8.42) and δ($H_β$-pyridyl) (δ = 7.21) in **4** ([D_8]THF) are nearly identical with those of BPEF (δ = 8.46 and 7.19, respectively), and it is impossible to estimate the number of repeating units n in **4** from the ^1H NMR spectroscopic data. Besides the pyridyl protons, the ferrocene protons (δ($H_α$-C_5H_4) = 4.61, δ($H_β$-C_5H_4) = 4.42) also display a similar chemical shift compared to those of free BPEF (δ = 4.57 and 4.37, respectively). The major difference is that the pyridyl protons in **4** show broad signals at room temperature. They become broader and shift to lower field [δ($H_α$) = 8.78, δ($H_β$) = 7.31] at +55 °C, but split to a doublet with peaks

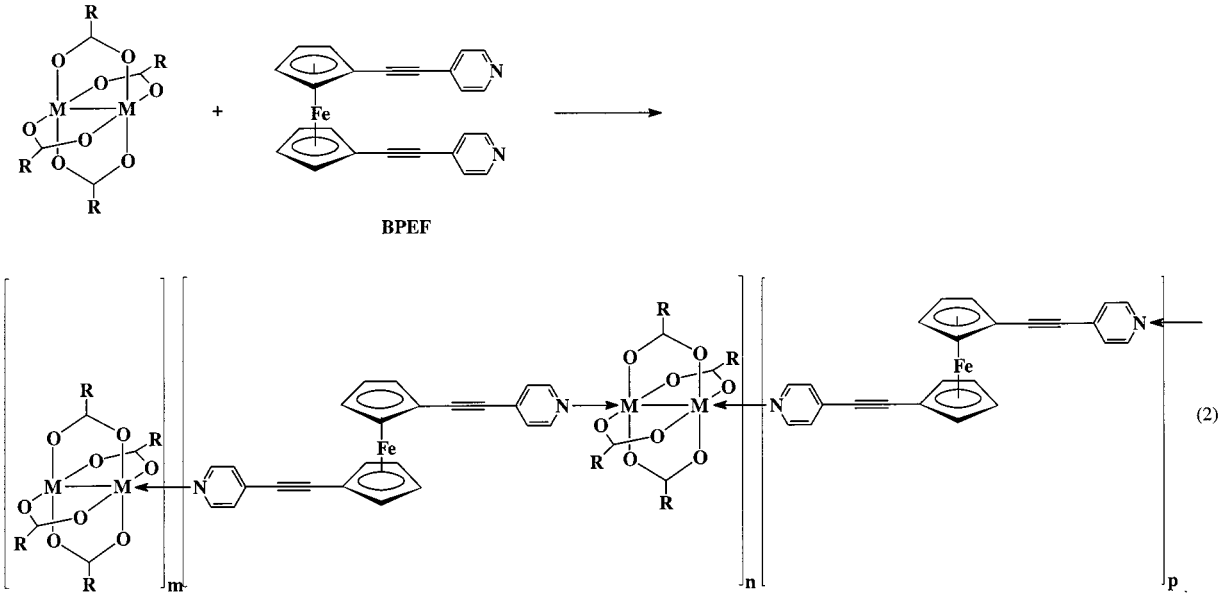

	M	R	m	n	p
4	Mo	CF_3	0	unknown	0
5	Rh	CH_3	1	ca. 3	0
6	Rh	CF_3	0	9-14	1

at δ = 8.38 and 7.20, respectively, at −80 °C. This behavior is probably due to a temperature-dependent fluxionality in the system. At lower temperatures the whole structure is more rigid. Increasing the temperature leads to significant thermal movements, causing a broadening of the signals. Free BPEF does not show temperature dependence in its NMR spectrum. The ^{13}C NMR chemical shift of the R−CO_2 carbon atom in complex **4** (δ = 166.7, [D_8]THF) is not significantly different from that in $Mo_2(O_2CCF_3)_4$ (δ = 167.0). Therefore it is assumed that the oligomer chain of complex **4** may be broken due to the combined effects of weak metal-axial ligand interactions and the relatively strong coordinating ability of the solvent THF which is present in high excess. It is known that the strong σ component found in Mo−Mo quadruple bonds ($\sigma^2\pi^4\delta^2$) prevents stronger binding of any low-lying orbitals at the axial positions.[2a] A huge excess of the coordinating solvent THF is therefore very likely to break the oligomer chain. It was reported that the dissolution of $[Ru_2(O_2C(CH_2)_6CH_3)_4(pyrazine)]_n$ in coordinating solvents such as THF and MeOH also resulted in breaking of the polymer chain.[3c] We have reported the preparation of $[Mo_2(\mu\text{-}O_2CCH_3)_2(\mu\text{-}dppma)_2(NC_5H_4\text{-}R)_2]^{2+}$ recently. A mixture of nitrile and pyridine ligated complexes is obtained if the reaction is conducted in acetonitrile instead of dichloromethane.[11] Chemical ionization mass spectrometry (CI-MS) measurements of oligomer **4** also indicate that the metal-axial ligand interaction is weak, showing two major peaks corresponding to $BPEF^+$ and $[Mo_2(O_2CCF_3)_4]^+$ but no parent oligomer ion.

At an onset temperature of ca. 273 °C the oligomer **4** breaks down, producing sublimed $Mo_2(O_2CCF_3)_4$ units. Further heating results in gradual decomposition of the residue and gives a residual weight of 30% at 800 °C under He atmosphere as shown by TGA analysis (Figure 4). It is to be noted, however, that the onset of sublimation for the starting material $[Mo_2(O_2CCH_3)_4]$ is more than 45 °C below the onset of the first decomposition step of compound **4** (226 °C). Derivative **4** is also significantly more stable than the analogous tetrameric complex **1** (see above). This not only proves that complex **4** is not merely a mixture of starting materials, but also explains why all the $[Mo_2(O_2CCH_3)_4]$ incorporated in derivative **4** does not sublime when the oligomeric structure breaks down. The temperature is already significantly above the sublimation temperature of the dimolybdenum precursor so that only part of it is still able to sublime; the remaining residue decomposes gradually.

In the solid state, compound **4** is stable in air for a couple of hours, but in solution it decomposes within 10 min when exposed to air. In order to obtain air stable organometallic oligomers of this type, $Rh_2(O_2CCH_3)_4$ and $Rh_2(O_2CCF_3)_4$ were employed to yield oligomers **5** and **6** as shown in Equation (2). It is additionally anticipated that $Rh_2(O_2CCF_3)_4$ leads to stronger metal-axial ligand interactions because it is a stronger Lewis acid than $Rh_2(O_2CCH_3)_4$. Accordingly, neither compound **5** nor complex **6** are soluble in any common solvents. THF and acetonitrile are unable to break the axial interactions between the dirhodium core and the BPEF ligands, in contrast to the case of compound **4**.

The IR spectra of **5** and **6** exhibit characteristic C≡C stretching vibrations at 2208 and 2210 cm^{-1}, respectively. Derivative **6** additionally shows the C−F stretching vibration at 1194 cm^{-1}. These data are comparable with those of free BPEF [ν(C≡C) = 2208 cm^{-1}] and free $Rh_2(O_2CCF_3)_4$ [ν(C−F) = 1190 cm^{-1}].

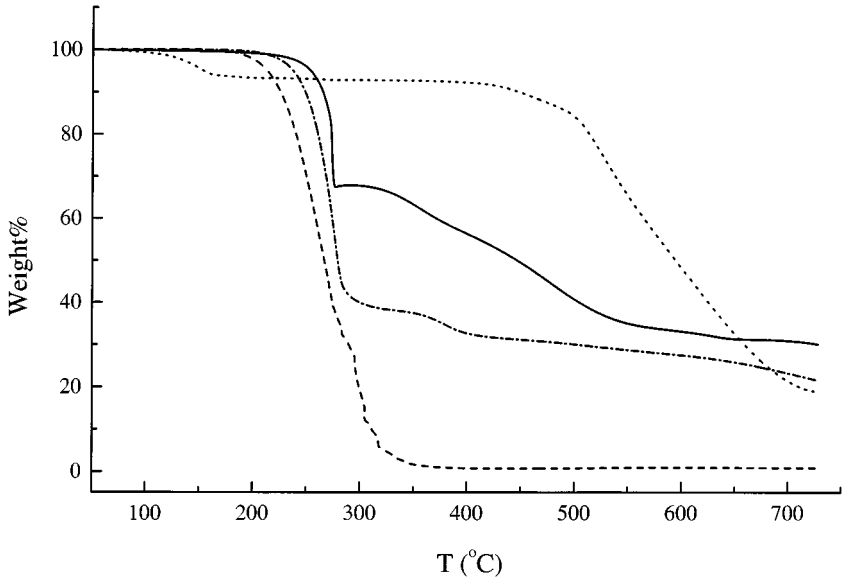

Figure 4. Plot of percent weight loss versus temperature for the thermal decomposition of $[Mo_2(O_2CCF_3)_4(BPEF)]_n$ (**4**, solid line), $Mo_2(O_2CCF_3)_4$ (dashed line), BPEF (dotted line), and $Mo_2(O_2CCF_3)_4(FPA)_2$ (**1**) (dashed-dotted line)

The poor solubility of complexes **5** and **6** prevents successful measurements of NMR spectra and the determination of the molecular mass in solution. However, the elemental analyses provide a rough way of estimating the number of repeating units and the terminal groups of the oligomers. The analytical results for complex **5** suggest the terminal groups are $Rh_2(O_2CCH_3)_4$ because the carbon content is much lower than that assumed for a stoichiometry $Rh_2(O_2CCH_3)_4$/BPEF = 1:1. The calculated elemental percentages are compared to the experimental data in Table 2. The percentages of H, N, and Fe are not sensitive enough to the extension of the oligomer chain, but those of C and Rh are quite informative. Taking the absolute error of the C analyses as 0.3%, and of the Rh analyses of 1%, the oligomer **5** has the composition of $[Rh_2(O_2CCH_3)_4]_{n+1}(BPEF)_n$ (n is around 3, most likely a mixture of oligomers with different lengths) and the average molecular mass is 2933. In the same manner, the composition of oligomer **6** is assumed to be $[Rh_2(O_2CCF_3)_4]_n(BPEF)_{n+1}$ (n = 9−14), the terminal groups are BPEF, and the molecular mass is in the range of 9803 to 15034 (Table 2). Considering the well-defined onset of sublimation for the complexes **4**−**6** (see below) it is unlikely that these derivatives still contain a significant amount of the starting materials (which can be removed easily by washing − see Experimental Section). Therefore the results obtained from elemental analysis should at least give a reliable estimation of the size of the oligomers.

The TGA profiles of complexes **5** and **6** are in principle similar to that of compound **4**. Oligomer **5** is thermally stable under a He atmosphere until the temperature reaches ca. 300 °C. Then the polymer structure breaks down and $Rh_2(O_2CCH_3)_4$ starts to sublime. Again, the longer chain of compound **5** is somewhat more stable than the tetranuclear model compound **2** (see above). Further heating results in gradual decomposition of the residue and gives a residual weight of 53% at 730 ° C. $Rh_2(O_2CCH_3)_4$ without any axial ligands has a sublimation onset temperature of about 20 °C (278 °C) below that of the oligomer **5**. Compound **6** is thermally stable under He below 320 °C. The residual weight is 28% at 730 °C. Despite the fact that the tetranuclear complex **3** is less stable than $Rh_2(O_2CCF_3)_4$, its oligomeric analogue **6** is more stable than this precursor (decomposition onset at 312 °C, see above). These data are additional proof of the significant interactions in the bimetallic complexes with the axial BPEF ligands.

Electrochemical Properties

The insolubility of oligomers **5** and **6** prevents investigation of their electrochemical properties in solution, but the properties of complex **4** were investigated by cyclic voltammetry. The usual solvent for the oxidation of ferrocene is dichloromethane due to its inertness towards ferrocenium-type ions. However, we employed acetonitrile and tetrahydrofuran for the measurements because complex **4** is much more soluble in these solvents. It is to be noted, however, that the data obtained are probably not representative of the oligomeric compound **4** but only of fragments of it and therefore have to be regarded with great caution. Dissolved complex **4** displays an irreversible $Fe^{3+/2+}$ oxidation at −0.20 V in THF, which is comparable to the parent BPEF (−0.22 V). The $Fe^{3+/2+}$ oxidation wave of BPEF (0.43 V) is still irreversible in MeCN. However, when the scan rate reaches 200 mV/s, a reversible curve with $E_{1/2}$ = 0.41 V is observed for compound **4** dissolved in acetonitrile. The fact that the oxidation potential for the dissolved derivative **4** is very close to that of free starting material supports the view of a breakdown of the oligomeric structure in solution.

Electronic Absorption Spectra

BPEF shows d-d transitions at 350 nm (3550 M^{-1} cm^{-1}) and 458 nm (870 M^{-1} cm^{-1}), as well as π-π* transition at 308 nm (16900 M^{-1} cm^{-1}) in CH_3CN. It is anticipated that

Table 2. Estimation of the terminal groups and the number of repeated units of oligomers **5** and **6** by elemental analyses

$[Rh_2(O_2CCH_3)_4]_{n+1}(BPEF)_n$ (n is ca. 3) **5** Ratio[a]	Formula	fw	C%	H%	N%	F%	Fe%	Rh%
Found			42.74	3.54	2.94	–	6.03	27.6
3:2	$C_{72}H_{68}Fe_2N_4O_{24}Rh_6$	2102.47	41.13	3.26	2.66	–	5.31	29.38
4:3	$C_{104}H_{96}Fe_3N_6O_{32}Rh_8$	2932.71	42.59	3.30	2.87	–	5.71	28.08
5:4	$C_{136}H_{124}Fe_4N_8O_{40}Rh_{10}$	3762.95	43.41	3.32	2.98	–	5.94	27.36
1:1	$(C_{32}H_{28}FeN_2O_8Rh_2)_n$	n×830.24	46.29	3.40	3.37	–	6.73	24.79

$[Rh_2(O_2CCF_3)_4]_n(BPEF)_{n+1}$ (n = 9–14) **6**

Ratio[b]	Formula	fw	C%	H%	N%	F%	Fe%	Rh%
Found			38.00	1.66	2.85	20.52	5.35	19.4
8:9	$C_{280}H_{144}F_{96}Fe_9N_{18}O_{64}Rh_{16}$	8757.26	38.40	1.66	2.88	20.83	5.74	18.80
9:10	$C_{312}H_{160}F_{108}Fe_{10}N_{20}O_{72}Rh_{18}$	9803.39	38.23	1.65	2.86	20.93	5.70	18.89
10:11	$C_{344}H_{176}F_{120}Fe_{11}N_{22}O_{80}Rh_{20}$	10846.24	38.06	1.64	2.84	21.02	5.67	18.98
11:12	$C_{376}H_{192}F_{132}Fe_{12}N_{24}O_{88}Rh_{22}$	11892.06	37.94	1.63	2.83	21.09	5.64	19.04
12:13	$C_{408}H_{208}F_{144}Fe_{13}N_{26}O_{96}Rh_{24}$	12937.88	37.88	1.62	2.81	21.15	5.62	19.09
13:14	$C_{440}H_{224}F_{156}Fe_{14}N_{28}O_{104}Rh_{26}$	13987.90	37.76	1.61	2.80	21.19	5.60	19.13
14:15	$C_{472}H_{240}F_{168}Fe_{15}N_{30}O_{112}Rh_{28}$	15034.02	37.71	1.61	2.80	21.23	5.57	19.17
15:16	$C_{504}H_{256}F_{180}Fe_{16}N_{32}O_{120}Rh_{30}$	16080.15	37.71	1.60	2.79	21.17	5.56	19.20
1:1	$(C_{32}H_{16}F_{12}FeN_2O_8Rh_2)_n$	n×1046.13	36.74	1.54	2.68	21.79	5.34	19.67

[a] Stoichiometry $Rh_2(O_2CCH_3)_4$:BPEF. – [b] Stoichiometry $Rh_2(O_2CCF_3)_4$:BPEF.

these absorption bands move to longer wavelengths and exhibit stronger extinction coefficients when BPEF forms an oligomer with $Mo_2(O_2CCF_3)_4$ in complex **4** for the same reasons as in the tetranuclear model complex **1**. However, the UV/Vis spectrum of dissolved complex **4** in CH_3CN does not show these features. The d-d and π-π* transitions of the dissolved derivative **4** are comparable to BPEF both in energy and in intensity, except that the d-d absorption around 350 nm appears as a shoulder of the π-π* absorption band of dissolved **4**. This behavior again supports the view that destruction of the oligomeric structure of **4** by the donor solvents occurs.

Conclusions

A new type of organometallic oligomer with the backbone consisting of bimetallic tetracarboxylates and a π-conjugated ferrocene derivative is easily generated by mixing the precursor compounds in solution at room temperature. The terminal groups and the number of repeating units are estimated by elemental analysis. The poor solubility of $[Rh_2(O_2CCH_3)_4]_{n+1}(BPEF)_n$ ($n \approx 3$) (**5**) and $[Rh_2(O_2CCF_3)_4]_n(BPEF)_{n+1}$ (n = 9–14) (**6**) prevents investigation of their electronic and electrochemical properties. The properties of dissolved $[Mo_2(O_2CCF_3)_4(BPEF)]_n$ (**4**) in MeCN and THF solutions are not related to the behavior of the real oligomer due to coordination competition between BPEF and the donor solvents. TGA studies prove the strength of the metal-axial interactions in the oligomeric complexes **4**–**6**. The electronic and electrochemical investigations of the tetranuclear model compounds indicate that the ferrocene units are electronically noncommunicating. Further research in this field will include modification of the tetracarboxylate ligands, bimetallic centers and ferrocene bridges in order to enhance the solubility of the oligomers and increase the electronic coupling within the oligomeric chains. Work in this direction is currently under way in our laboratory.

Experimental Section

General: All preparations and manipulations were carried out under an oxygen- and water-free argon atmosphere using standard Schlenk techniques. Solvents were dried by standard procedures, distilled, and stored under argon over 4-Å molecular sieves. $Mo_2(O_2CCF_3)_4$,[2e] $Rh_2(O_2CCH_3)_4$,[11] and $Rh_2(O_2CCF_3)_4$[12] were prepared according to the literature methods. – Elemental analyses were performed at the Mikroanalytisches Labor of the TU München in Garching. – ^1H and ^{13}C NMR were recorded by a Jeol JNM GX-400 spectrometer. – IR spectra were obtained on a Perkin–Elmer FT-IR spectrometer using KBr pellets as IR matrix. – Electronic absorption spectra were recorded using a Perkin–Elmer Lambda 2 UV/Vis spectrometer. – Cyclic voltammograms were recorded with a computer-controlled Model 173 Potentiostat/galvanostat (EG&G Princeton Applied Research) in argon-saturated and dry solutions with tetrabutylammonium hexafluorophosphate (TBAH, 0.1 M) as supporting electrolyte. The working electrode was platinum and the reference electrode silver wire. Potentials are quoted vs. the ferrocene/ferrocenium couple as internal standard. – TGA was performed using a Perkin–Elmer TGA 7 Thermogravimetric Analyzer with a heating rate of 15 °C/min.

Ferrocenyl-4-pyridylacetylene (FPA): Synthesized from ferrocenylacetylene[13] and 4-bromopyridine hydrochloride using a modified literature procedure.[14] Decomposes at 154 °C. – $C_{17}H_{13}FeN$ (287.14): calcd. C 71.11, H 4.56, N 4.88; found C 71.25, H 4.47, N 4.59. – Positive FAB-MS: m/z = 288 $[FPA + H^+]^+$. – Selected IR (KBr): $\tilde{\nu}$ = 2210 s (C≡C), 1636 m, 1594 vs, 1536 m, 1455 m, 1411 m, 1103 m, 1040 m, 1023 m, 1004 m, 987 m, 927 m, 817 vs, 538 m, 499 s, 483 s cm^{-1}. – ^1H NMR (CD_2Cl_2, room temp.): δ = 4.25 (s, 5 H, C_5H_5), 4.31 (t, 2 H, H_β-C_5H_4), 4.54 (t, 2 H, H_α-C_5H_4), 7.32 (d, 2 H, H_β-C_5H_4N), 8.53 (d, 2 H, H_α-C_5H_4N). – ^{13}C NMR

(CD_2Cl_2, room temp.): δ = 69.9, 70.4, 72.1 (C_5H_5 & C_5H_4), 83.6 (C_5H_4CC), 94.3 (CCC_5H_4N), 125.5 (C_β-C_5H_4N), 132.3 (C_γ-C_5H_4N), 150.1 (C_α-C_5H_4N).

1,1′-Bis(4-pyridylethynyl)ferrocene (BPEF): Synthesized by a modified literature procedure for 1,1′-bis(phenylethynyl)ferrocene.[10] A mixture of 1,1′-diiodoferrocene[15] (1.0 g, 2.3 mmol), 4-ethynylpyridine[16] (0.60 g, 5.8 mmol), $Pd(PPh_3)_4$ (0.10 g, 0.090 mmol), CuI (0.018 g, 0.090 mmol), and (iPr)$_2$NH (40 mL) was heated at reflux for 24 h. The solvent was removed under vacuum, and the residue extracted with H_2O/CH_2Cl_2. The organic layer was washed with H_2O, dried with $MgSO_4$, and chromatographed on a SiO_2 (70−220 mesh) column. Successive elution with CH_2Cl_2 and CH_2Cl_2/THF (1:1) led to the development of three bands. The third band in reddish-orange color afforded 0.70 g (89%) of the product. Decomposes at 155 °C. − $C_{24}H_{16}FeN_2$ (387.85): calcd. C 74.26, H 4.13, N 7.22; found C 73.98, H 4.37, N 7.01. − positive FAB-MS: *m/z*: 389 [BPEF + H^+]$^+$. − selected IR (KBr): $\tilde{\nu}$ = 2208 s (C≡C), 1633 m, 1592 vs, 1536 m, 1405 m, 1261 s, 1097 s, 1030 s, 997 m, 932 m, 817 vs, 801 vs, 540 m, 498 s cm^{-1}. − ^{1}H NMR ($CDCl_3$, room temp.): δ = 4.37 (t, 4 H, H_β-C_5H_4), 4.57 (t, 4 H, H_α-C_5H_4), 7.19 (d, 4 H, H_β-C_5H_4N), 8.46 (d, 4 H, H_α-C_5H_4N). − ^{13}C NMR ($CDCl_3$, room temp.): δ = 68.0, 71.4, 73.4 (C_5H_4), 84.5 (C_5H_4CC), 92.4 (CCC_5H_4N), 125.2 (C_β-C_5H_4N), 131.8 (C_γ-C_5H_4N), 149.6 (C_α-C_5H_4N).

$Mo_2(O_2CCF_3)_4(FPA)_2$ (1): A CH_2Cl_2 solution (25 mL) containing $Mo_2(O_2CCF_3)_4$ (0.10 g, 0.16 mmol) and FPA (0.10 g, 0.35 mmol) was stirred at room temperature for 2 h. The solvent was removed under oil pump vacuum and the residue was washed with *n*-hexane. Yield: 0.16 g, 82%. Slow evaporation of the diethyl ether solution of **1** gave crystals suitable for single crystal X-ray analysis. − $C_{42}H_{26}F_{12}Fe_2Mo_2N_2O_8$ (1218.23): calcd. C 41.41, H 2.15, N 2.30; found C 41.16, H 2.24, N 2.19. − Selected IR (KBr): $\tilde{\nu}$ = 2207 s (C≡C), 1601 vs, 1421 m, 1220 vs, 1193 vs. (C−F), 1170 vs, 1155 vs, 1004 s, 925 m, 856 m, 816 s, 779 m, 730 s, 596 m, 538 m, 499 m cm^{-1}. − ^{1}H NMR (CD_2Cl_2, room temp.): δ = 4.23 (s, 10 H, C_5H_5), 4.33 (t, 4 H, H_β-C_5H_4), 4.53 (t, 4 H, H_α-C_5H_4), 7.24 (d, 4 H, H_β-C_5H_4N), 8.03 (d, 4 H, H_α-C_5H_4N). − ^{13}C NMR (CD_2Cl_2, room temp.): δ = 70.2, 70.5, 72.3 (C_5H_5 & C_5H_4), 83.2 (C_5H_4CC), 126.0 (C_β-C_5H_4N), 149.2 (C_α-C_5H_4N), 166.6 (CO_2).

$Rh_2(O_2CCH_3)_4(FPA)_2$ (2): A solution of FPA (0.14 g, 0.50 mmol) in THF (10 mL) was added to a THF solution (30 mL) of $Rh_2(O_2CCH_3)_4$ (0.10 g, 0.23 mmol). The orange precipitate was collected and washed with Et_2O after being stirred at room temperature for 2 h. Yield: 0.18 g, 78%. − $C_{42}H_{38}Fe_2N_2O_8Rh_2$ (1016.28): calcd. C 49.64, H 3.77, N 2.76; found C 49.51, H 3.79, N 2.46. − Selected IR (KBr): $\tilde{\nu}$ = 2205 vs (C≡C), 1593 vs, 1450 m, 1429 vs, 1344 m, 1217 m, 1171 m, 1107 m, 1061 m, 1012 m, 925 m, 826 s, 694 s, 628 m, 600 m, 541 m, 500 s, 483 m, 446 m cm^{-1}. − ^{1}H NMR (CD_2Cl_2, room temp.): δ = 1.88 (s, 12 H, CH_3), 4.31 (s, 10 H, C_5H_5), 4.38 (t, 4 H, H_β-C_5H_4), 4.63 (t, 4 H, H_α-C_5H_4), 7.72 (d, 4 H, H_β-C_5H_4N), 9.11 (s, br, 4 H, H_α-C_5H_4N). − ^{13}C NMR (CD_2Cl_2, room temp.): δ = 30.1 (CH_3), 70.2, 70.6, 72.4 (C_5H_5 & C_5H_4), 126.9 (C_β-C_5H_4N), 150.6 (C_α-C_5H_4N), 191.4 (CO_2).

$Rh_2(O_2CCF_3)_4(FPA)_2$ (3): A solution of FPA (0.096 g, 0.33 mmol) in Et_2O (20 mL) was added to a solution of $Rh_2(O_2CCF_3)_4$ (0.10 g, 0.15 mmol) in Et_2O (10 mL). The orange precipitate was collected and washed with Et_2O after being stirred at room temperature for 2 h. Yield: 0.090 g, 49%. − $C_{42}H_{26}F_{12}Fe_2N_2O_8Rh_2$ (1232.16): calcd. C 40.94, H 2.13, N 2.27; found C 40.50, H 1.98, N 2.16. − selected IR (KBr): $\tilde{\nu}$ = 2206 vs (C≡C), 1662 vs, 1604 vs, 1456 m, 1424 m, 1223 vs, 1193 vs (C−F), 1172 vs, 1016 m, 925 m, 858 m, 818 s, 786 m, 738 s, 603 m, 540 m, 501 m cm^{-1}. − ^{1}H NMR ([D$_8$]THF, room temp.): δ = 4.26 (s, 10 H, C_5H_5), 4.39 (s, 4 H, H_β-C_5H_4), 4.61 (s, 4 H, H_α-C_5H_4), 7.46 (d, 4 H, H_β-C_5H_4N), 8.27 (d, 4 H, H_α-C_5H_4N). − ^{13}C NMR ([D$_8$]THF, room temp.): δ = 70.1, 72.8 (C_5H_5 & C_5H_4), 83.5 (C_5H_4CC), 99.6 (CCC_5H_4N), 113.3 (CF_3), 126.6 (C_β-C_5H_4N), 135.6 (C_γ-C_5H_4N), 152.3 (C_α-C_5H_4N), 175.7 (CO_2).

$[Mo_2(O_2CCF_3)_4(BPEF)]_n$ (4): A CH_2Cl_2 solution (10 mL) of BPEF (0.050 g, 0.13 mmol) was added to a CH_2Cl_2 solution (10 mL) of $Mo_2(O_2CCF_3)_4$ (0.071 g, 0.11 mmol), immediately giving an orange precipitate. After being stirred at room temperature for 2 h, the precipitate was collected and washed with Et_2O. Yield: 0.095 g (84%). − $(C_{32}H_{16}F_{12}FeN_2Mo_2O_8)_n$ ($n \times$ 1032.2): calcd. C 37.24, H 1.56, F 22.09, Fe 5.41, Mo 18.90, N 2.71; found C 37.56, H 1.50, F 23.51, Fe 3.88, Mo 19.24, N 2.67. − Selected IR (KBr): $\tilde{\nu}$ = 2211 m (C≡C), 1633 m, 1603 vs, 1424 m, 1222 vs, 1193 vs (C−F), 1159 vs, 1002 m, 856 m, 824 m, 780 m, 731 vs, 595 s, 502 m cm^{-1}. − ^{1}H NMR ([D$_8$]THF, room temp.): δ = 4.42 (s, 4 H, H_β-C_5H_4), 4.61 (s, 4 H, H_α-C_5H_4), 7.21 (s, 4 H, H_β-C_5H_4N), 8.42 (s, br, 4 H, H_α-C_5H_4N). − ^{13}C NMR ([D$_8$]THF, room temp.): δ = 72.3, 74.2 (C_5H_4), 85.2 (C_5H_4CC), 93.0 (CCC_5H_4N), 114.6 (CF_3), 126.0 (C_β-C_5H_4N), 132.5 (C_γ-C_5H_4N), 150.6 (C_α-C_5H_4N), 166.7 (CO_2).

$[Rh_2(O_2CCH_3)_4]_{n+1}(BPEF)_n$ ($n \approx$ 3) (5): A THF solution (15 mL) of $Rh_2(O_2CCH_3)_4$ (0.057 g, 0.13 mmol) was added to a THF solution (5 mL) of BPEF (0.050 g, 0.13 mmol). The orange precipitate was collected and washed with THF after being stirred at room temperature for 2 h. Yield: 0.10 g, 93%. − $C_{104}H_{96}Fe_3N_6O_{32}Rh_8$ (2932.71): calcd. C 42.59, H 3.30, Fe 5.71, N 2.87, Rh 28.07; found C 42.74, H 3.54, Fe 6.03, N 2.94, Rh 27.6. − selected IR (KBr): $\tilde{\nu}$ = 2208 m (C≡C), 1592 vs, 1500 m, 1429 vs, 1346 m, 1216 m, 1046 m, 1027 m, 1010 m, 827 m, 696 s, 628 m, 555 m, 478 m cm^{-1}.

$[Rh_2(O_2CCF_3)_4]_n(BPEF)_{n+1}$ (n = 9−14) (6): A CH_2Cl_2 solution (10 mL) of $Rh_2(O_2CCF_3)_4$ (0.039 g, 0.059 mmol) was quickly added to a CH_2Cl_2 solution (10 mL) of BPEF (0.023 g, 0.059 mmol). The reddish-orange precipitate was collected after 1 h and washed with Et_2O. Yield: 0.055 g, 86%. − For calculated analytical data refer to Table 2; found C 38.00, H 1.66, F 20.52, Fe 5.35, N 2.85, Rh 19.4. − Selected IR (KBr): $\tilde{\nu}$ = 2210 m (C≡C), 1666 vs, 1606 s, 1426 m, 1222 vs, 1194 vs (C−F), 1169 vs, 1016 m, 858 m, 828 m, 786 m, 738 s, 540 m, 503 m cm^{-1}.

X-ray Crystallography: Crystal data and details of the structure determination are presented in Table 3. A clear red-brown plate (0.25 × 0.15 × 0.05 mm) was employed for the analysis. Preliminary examination and data collection were carried out on a Kappa CCD area detecting diffraction system (NONIUS; MACH^3) equipped with a rotating anode and graphite monochromated Mo-K_α radiation (NONIUS; FR 591). The unit cell parameters were obtained by full-matrix least-squares refinements of 31046 reflections. Data collection were performed at 153 K (exposure time: 60 s per frame; 9 sets, and Ω-scans, Δ/ΔΩ: 1°; *d*x: 40.0 mm). A total number of 19385 reflections were collected. Raw data were corrected for Lorentz and polarization effects, corrected for absorption and decay effects and scaled with the program DENZO-SMN. After merging (R_{int} = 0.0184) a sum of 4089 independent reflections remained and were used for all calculations. All "heavy atoms" of the asymmetric unit were refined anisotropically. All hydrogen atoms were located in the difference Fourier map and refined with individual isotropic temperature parameters. Full-matrix least-squares refinements were carried out by minimizing $\Sigma w(F_o^2 - F_c^2)^2$ with SHELX-97 weighting scheme and stopped at shift/err < 0.001. Neutral atom scattering factors for all atoms and anomalous dispersion

corrections for the non-hydrogen atoms were taken from *International Tables for Crystallography.* All calculations were performed on a DEC 3000 AXP workstation and an Intel Pentium II PC, with the STRUX system, including the programs PLATON, SIR92, and SHELX-97.[17]

Table 3. Selected crystallographic data for $[Mo_2(O_2CCF_3)_4(FPA)_2]$ (**1**)

Empirical formula	$C_{42}H_{26}F_{12}Fe_2Mo_2N_2O_8$
fw	1218.23
Crystal system	triclinic
Space group	$P\bar{1}$
a [pm]	1034.29(2)
b [pm]	1040.16(3)
c [pm]	1175.90(3)
α [deg]	100.876(1)
β [deg]	115.989(1)
γ [deg]	95.447(1)
V [10^6 pm^3]	1093.88(5)
Z	1
$\rho_{calcd.}$ [g cm^{-3}]	1.849
F_{000}	600
μ [mm^{-1}]	1.316
Θ range [deg]	2.04 to 25.58
Data collcd (*h,k,l*)	±12, ±12, ±14
No. of reflections collected	19385
No. of independent reflections (all data)	4089
No. of observed reflections [$I_o > 2\sigma(I_o)$]	3796
No. of parameters refined	359
$R1$[a] [$I_o > 2\sigma(I_o)$/all data]	0.0265/0.0291
$wR2$[b]	0.0662
GOF[c]	1.034
Weights *a*/*b*[d]	0.0241/1.4782
$\Delta\rho_{max/min}$ [e Å^{-3}]	1.07/−0.54

[a] $R1 = \Sigma(||F_o| - |F_c||)/\Sigma|F_o|$. – [b] $wR2 = [\Sigma w (F_o^2 - F_c^2)^2/\Sigma w (F_o^2)^2]^{1/2}$. – [c] $GOF = [\Sigma w (F_o^2 - F_c^2)^2/(NO - NV)]^{1/2}$. – [d] $w = 1/[\sigma^2(F_o^2) + (a*P)^2 + b*P]$ with P: [max (0 or F_o^2) + $2F_c^2$]

Crystallographic data (excluding structure factors) for the structures reported in this paper have been deposited with the Cambridge Crystallographic Data Centre as supplementary publication no. CCDC-150833 (**1**). Copies of the data can be obtained free of charge on application to CCDC, 12 Union Road, Cambridge CB2 1EZ, UK [Fax: (internat.) +44-1223/336-033; E-mail: deposit@ccdc.cam.ac.uk].

Acknowledgments

W.-M. X. thanks the Alexander von Humboldt Foundation for a postdoctoral research associate fellowship. Professor W. A. Herrmann is acknowledged for continuous support of our work. Professor D. Wabner and Mr. T. Görlach are acknowledged for helpful discussions concerning cyclovoltammetry and DPV measurement.

[1] [1a] *Inorganic materials* (Eds.: D. W. Bruce, D. O'Hare), Wiley, **1992**. – [1b] *Extended Linear Chain Compounds*, *Vol. 1–3*, (Ed.: J. S. Miller), Plenum, New York, **1982**. – [1c] L. Oriol, J. L. Serrano, *Adv. Mater.* **1995**, *7*, 348. – [1d] N. G. Connelly, W. E. Geiger, *Adv. Organomet. Chem.* **1984**, *23*, 1. – [1e] N. G. Connelly, W. E. Geiger, *Adv. Organomet. Chem.* **1985**, *24*, 87. – [1f] M. H. Chisholm, *Acc. Chem. Res.* **2000**, *33*, 53 and references cited therein.

[2] [2a] *Multiple Bonds Between Metal Atoms* (Eds.: F. A. Cotton, R. A. Walton), 2nd edition, Oxford University Press, London, **1993**. – [2b] F. A. Cotton, T. R. Felthouse, *Inorg. Chem.* **1980**, *19*, 328. – [2c] F. A. Cotton, T. R. Felthouse, *Inorg. Chem.* **1981**, *20*, 600. – [2d] F. A. Cotton, Y. Kim, T. Ren, *Inorg. Chem.* **1992**, *31*, 2723. – [2e] F. A. Cotton, J. G. Norman, *J. Coord. Chem.* **1971**, *1*, 161.

[3] [3a] M. Handa, K. Kasamatsu, K. Kasuge, M. Mikuriya, T. Fujii, *Chem. Lett.* **1990**, 1753. – [3b] B. Morison, R. C. Hughes, Z. G. Soos, *Acta Crystallogr.* **1975**, *B31*, 762. – [3c] J. L. Wesemann, M. H. Chrisholm, *Inorg. Chem.* **1997**, *36*, 3258. – [3d] M. Handa, H. Matsumoto, D. Yashioka, R. Nukada, M. Mikuriya, I. Hiromitsu, K. Kasuge, *Bull. Chem. Soc. Jpn.* **1998**, *71*, 1811. – [3e] X. Ouyang, C. Campana, K. R. Dunbar, *Inorg. Chem.* **1996**, *35*, 7188. – [3f] M. C. Kerby, B. W. Eichhorn, J. A. Creighton, K. P. C. Vollhardt, *Inorg. Chem.* **1990**, *29*, 1319.

[4] [4a] A. Togni, M. Hobi, G. Rihs, G. Rist, A. Albinati, P. Zanello, D. Zech, H. Keller, *Organometallics* **1994**, *13*, 1224. – [4b] R. Rulkens, A. J. Lough, I. Manners, S. R. Lovelace, C. Grant, W. E. Geiger, *J. Am. Chem. Soc.* **1996**, *118*, 12683. – [4c] F. F. Debiani, T. Gmeinwieser, E. Herdtweck, F. Jäkle, F. Laschi, M. Wagner, P. Zanello, *Organometallics* **1997**, *16*, 4776. – [4d] F. F. Debiani, F. Jäkle, M. Spiegler, M. Wagner, P. Zanello, *Inorg. Chem.* **1997**, *36*, 2103. – [4e] M. Fontani, F. Peters, W. Scherer, W. Wachter, M. Wagner, P. Zanello, *Eur. J. Inorg. Chem.* **1998**, 1453. – [4f] M. Grosche, E. Herdtweck, F. Peters, M. Wagner, *Organometallics* **1999**, *18*, 4669.

[5] [5a] R. W. Wagner, P. A. Brown, T. E. Johnson, J. S. Lindsey, *J. Chem. Soc., Chem. Commun.* **1991**, 1463. – [5b] E. C. Constable, *Angew. Chem. Int. Ed. Engl.* **1991**, *30*, 407.

[6] See, for example: – [6a] K. L. Kott, D. A. Higgins, R. J. McMahon, R. M. Corn, *J. Am. Chem. Soc.* **1993**, *115*, 5342. – [6b] Z. Yuan, N. J. Taylor, Y. Sun, T. B. Marder, I. D. Williams, L.-T. Cheng, *J. Organomet. Chem.* **1993**, *449*, 27. – [6c] Z. Yuan, G. Stringer, I. R. Jobe, D. Kreller, K. Scott, L. Koch, N. J. Taylor, T. B. Marder, *J. Organomet. Chem.* **1993**, *452*, 115. – [6d] Benito, J. Cano, R. Martinez-Manez, J. Paya, J. Soto, M. Julve, F. Loret, M. D. Marcos, E. Sinn, *J. Chem. Soc., Dalton Trans.* **1993**, 1999.

[7] P. Nguyen, P. Gómez-Elipe, I. Manners, *Chem. Rev.* **1999**, *99*, 1515, and references therein.

[8] 3d Search and Research Using the Cambridge Structural Database; F. H. Allen, O. Kennard, *Chemical Design Automation News* **1993**, *8*, 1 and 31–37. The refcodes are as follows: BEYFIU, BURTEN, BURTIR (2x), MOTFAC, REPPUX, TFACMO, TIZWUU, TUFVIZ, VOZCIW, WEJZIU.

[9] T. H. Barr, W. E. Watts, *J. Organomet. Chem.* **1968**, *15*, 177.

[10] [10a] W.-M. Xue, F. E. Kühn, G. Zhang, E. Herdtweck, *J. Organomet. Chem.* **2000**, *596*, 177. – [10b] W.-M. Xue, F. E. Kühn, G. Zhang, E. Herdtweck, G. Raudaschl-Sieber, *J. Chem. Soc., Dalton Trans.* **1999**, 4103.

[11] G. A. Rempel, P. Legzdius, H. Smith, G. Wilkinson, *Inorg. Synth.* **1972**, *13*, 90.

[12] J. Kitchens, J. L. Bear, *Thermochimica Acta* **1970**, *1*, 537.

[13] M. Rosenblum, N. Brawn, J. Papenmeier, M. Applebaum, *J. Organomet. Chem.* **1966**, *6*, 173.

[14] J. T. Lin, J. J. Wu, C.-S. Li, Y. S. Wen, K.-J. Lin, *Organometallics* **1996**, *15*, 5028.

[15] R. F. Kovar, M. D. Rausch, H. Rosenberg, *Organomet. Chem. Synth.* **1970/1971**, *1*, 173.

[16] L. D. Ciana, A. Haim, *J. Heterocyclic Chem.* **1984**, *21*, 607.

[17] Data collection and data reduction: [17a] B. V. Nonius, NONIUS MACH3 *Operating System Version 5.1*, Delft, The Netherlands, **1994**. – [17b] Z. Otwinowski, W. Minor, *Methods in Enzymology* **1997**, *276*, 307. – [17c] *Tables for Crystallography*, Vol. C, Tables 6.1.1.4 (pp. 500–502), 4.2.6.8 (pp. 219–222), and 4.2.4.2 (pp. 193–199), Ed. A. J. C. Wilson, Kluwer Academic Publishers, Dordrecht, The Netherlands, **1992**. – [17d] G. Artus, W. Scherer, T. Priermeier, E. Herdtweck, *STRUX-V, A Program System to Handle X-ray Data*, TU München, Germany, **1997**. Structure solution: [17e] SIR92: A. Altomare, G. Cascarano, C. Giacovazzo, A. Guagliardi, M. C. Burla, G. Polidori, M. Camalli, , *J. Appl. Cryst.* **1994**, *27*, 435. Structure refinement: [17f] G. M. Sheldrick, *SHELXL-97*, University of Göttingen, Göttingen, Germany, **1998**. Graphics: [17g] A. L. Spek, *PLATON, A Multipurpose Crystallographic Tool*, Utrecht University, Utrecht, The Netherlands, **1999**.

Received April 17, 2000
[I00153]